Geometrical shape design of nanophotonic surfaces for thin film solar cells

W. I. Nam, Y. J. Yoo and Y. M. Song*

Department of Electronics Engineering, Pusan National University, 2 Busandaehakro 63 beon-gil, Geumjeong-gu, Busan 609-735, South Korea

**ymsong81@gmail.com*

Abstract: We present the effect of geometrical parameters, particularly shape, on optical absorption enhancement for thin film solar cells based on crystalline silicon (*c*-Si) and gallium arsenide (GaAs) using a rigorous coupled wave analysis (RCWA) method. It is discovered that the "sweet spot" that maximizes efficiency of solar cells exists for the design of nanophotonic surfaces. For the case of ultrathin, rod array is practical due to the effective optical resonances resulted from the optimum geometry whereas parabola array is viable for relatively thicker cells owing to the effective graded index profile. A specific value of thickness, which is the median value of other two devices tailored by rod and paraboloid, is optimized by truncated shape structure. It is therefore worth scanning the optimum shape of nanostructures in a given thickness in order to achieve high performance.

OCIS codes: (040.5350) Photovoltaic; (080.2740) Geometric optical design; (310.6628) Subwavelength structures, nanostructures; (350.6050) Solar energy.

References and links

1. A. Polman and H. A. Atwater, "Photonic design principles for ultrahigh-efficiency photovoltaics," Nat. Mater. **11**(3), 174–177 (2012).
2. H. A. Atwater and A. Polman, "Plasmonics for improved photovoltaic devices," Nat. Mater. **9**(3), 205–213 (2010).
3. S. B. Mallick, N. P. Sergeant, M. Agrawal, J.-Y. Lee, and P. Peumans, "Coherent light trapping in thin-film photovoltaics," MRS Bull. **36**(6), 453–460 (2011).
4. M. A. Green, K. Emery, Y. Hishikawa, W. Warta, and E. D. Dunlop, "Solar cell efficiency tables (Version 45)," Prog. Photovolt. Res. Appl. **23**(1), 1–9 (2015).
5. E. Moulin, U. W. Paetzold, H. Siekmann, J. Worbs, A. Bauer, and R. Carius, "Study of thin-film silicon solar cell back reflectors and potential of detached reflectors," Energy Procedia **10**, 106–110 (2011).
6. J. Zhu, C. M. Hsu, Z. Yu, S. Fan, and Y. Cui, "Nanodome solar cells with efficient light management and self-cleaning," Nano Lett. **10**(6), 1979–1984 (2010).
7. X. Sheng, S. G. Johnson, L. Z. Broderick, J. Michel, and L. C. Kimerling, "Integrated photonic structures for light trapping in thin-film Si solar cells," Appl. Phys. Lett. **100**(11), 111110 (2012).
8. J. Zhu, Z. Yu, G. F. Burkhard, C. M. Hsu, S. T. Connor, Y. Xu, Q. Wang, M. McGehee, S. Fan, and Y. Cui, "Optical absorption enhancement in amorphous silicon nanowire and nanocone arrays," Nano Lett. **9**(1), 279–282 (2009).
9. J. Li, H. Yu, S. M. Wong, G. Zhang, X. Sun, P. G.-Q. Lo, and D. L. Kwong, "Si nanopillar array optimization on Si thin films for solar energy harvesting," Appl. Phys. Lett. **95**(3), 033102 (2009).
10. X. Sheng, L. Z. Broderick, and L. C. Kimerling, "Photonic crystal structures for light trapping in thin-film Si solar cells: Modeling, process and optimizations," Opt. Commun. **314**, 41–47 (2014).
11. B. Hua, B. Wang, M. Yu, P. W. Leu, and Z. Fan, "Rational geometrical design of multi-diameter nanopillars for efficient light harvesting," Nano Energy **2**(5), 951–957 (2013).
12. J. Buencuerpo, L. E. Munioz-Camuniez, M. L. Dotor, and P. A. Postigo, "Optical absorption enhancement in a hybrid system photonic crystal - thin substrate for photovoltaic applications," Opt. Express **20**, A452–A464 (2012).
13. E. Garnett and P. Yang, "Light trapping in silicon nanowire solar cells," Nano Lett. **10**(3), 1082–1087 (2010).
14. G. Mariani, Y. Wang, P.-S. Wong, A. Lech, C.-H. Hung, J. Shapiro, S. Prikhodko, M. El-Kady, R. B. Kaner, and D. L. Huffaker, "Three-dimensional core-shell hybrid solar cells via controlled in situ materials engineering," Nano Lett. **12**(7), 3581–3586 (2012).
15. M.-A. Tsai, P.-C. Tseng, H.-C. Chen, H.-C. Kuo, and P. Yu, "Enhanced conversion efficiency of a crystalline silicon solar cell with frustum nanorod arrays," Opt. Express **19**(1), A28–A34 (2011).

#261695 Received 22 Mar 2016; revised 8 May 2016; accepted 11 May 2016; published 25 May 2016

16. F. J. Bezares, J. P. Long, O. J. Glembocki, J. Guo, R. W. Rendell, R. Kasica, L. Shirey, J. C. Owrutsky, and J. D. Caldwell, "Mie resonance-enhanced light absorption in periodic silicon nanopillar arrays," Opt. Express **21**(23), 27587–27601 (2013).
17. B. Wang and P. W. Leu, "Tunable and selective resonant absorption in vertical nanowires," Opt. Lett. **37**(18), 3756–3758 (2012).
18. Y. M. Song, J. S. Yu, and Y. T. Lee, "Antireflective submicrometer gratings on thin-film silicon solar cells for light-absorption enhancement," Opt. Lett. **35**(3), 276–278 (2010).
19. Y. Kanamori, M. Sasaki, and K. Hane, "Broadband antireflection gratings fabricated upon silicon substrates," Opt. Lett. **24**(20), 1422–1424 (1999).
20. H. L. Chen, S. Y. Chuang, C. H. Lin, and Y. H. Lin, "Using colloidal lithography to fabricate and optimize sub-wavelength pyramidal and honeycomb structures in solar cells," Opt. Express **15**(22), 14793–14803 (2007).
21. A. Asadollahbaik, S. A. Boden, M. D. B. Charlton, D. N. R. Payne, S. Cox, and D. M. Bagnall, "Reflectance properties of silicon moth-eyes in response to variations in angle of incidence, polarisation and azimuth orientation," Opt. Express **22**(S2), A402–A415 (2014).
22. Z. Yu, H. Gao, W. Wu, H. Ge, and S. Y. Chou, "Fabrication of large area subwavelength antireflection structures on Si using trilayer resist nanoimprint lithography and liftoff," J. Vac. Sci. Technol. B **21**(6), 2874–2877 (2003).
23. J. W. Leem, Y. M. Song, and J. S. Yu, "Broadband wide-angle antireflection enhancement in AZO/Si shell/core subwavelength grating structures with hydrophobic surface for Si-based solar cells," Opt. Express **19**(S5), A1155–A1164 (2011).
24. H. Sai, H. Fujii, K. Arafune, Y. Ohshita, Y. Kanamori, H. Yugami, and M. Yamaguchi, "Wide-angle antireflection effect of subwavelength structures for solar cells," Jpn. J. Appl. Phys. **46**(6A), 3333–3336 (2007).
25. Q. Chen, G. Hubbard, P. A. Shields, C. Liu, D. W. E. Allsopp, W. N. Wang, and S. Abbott, "Broadband moth-eye antireflection coatings fabricated by low-cost nanoimprinting," Appl. Phys. Lett. **94**(26), 263118 (2009).
26. D. F. Edwards, "Silicon (Si)," in *Handbook of Optical Constants of Solids*, E. D. Palik, ed. (Academic Press, 1985).
27. J. B. Theeten, D. E. Aspnes, and R. P. H. Chang, "A new resonant ellipsometric technique for characterizing the interface between GaAs and its plasma-grown oxide," J. Appl. Phys. **49**(12), 6097–6102 (1978).
28. H. Park, D. Shin, G. Kang, S. Baek, K. Kim, and W. J. Padilla, "Broadband optical antireflection enhancement by integrating antireflective nanoislands with silicon nanoconical-frustum arrays," Adv. Mater. **23**(48), 5796–5800 (2011).
29. J. W. Leem, Y. M. Song, and J. S. Yu, "Broadband antireflective germanium surfaces based on subwavelength structures for photovoltaic cell applications," Opt. Express **19**(27), 26308-26317 (2011).
30. A. D. Rakić, A. B. Djurišic, J. M. Elazar, and M. L. Majewski, "Optical properties of metallic films for vertical-cavity optoelectronic devices," Appl. Opt. **37**(22), 5271–5283 (1998).
31. X. Meng, G. Gomard, O. El Daif, E. Drouard, R. Orobtchouk, A. Kaminski, A. Fave, M. Lemiti, A. Abramov, P. Roca i Cabarrocas, and C. Seassal, "Absorbing photonic crystals for silicon thin-film solar cells: design, fabrication and experimental investigation," Sol. Energy Mater. Sol. Cells **95**, S32–S38 (2011).
32. G. Gomard, X. Meng, E. Drouard, K. El Hajjam, E. Gerelli, R. Peretti, A. Fave, R. Orobtchouk, M. Lemiti, and C. Seassal, "Light harvesting by planar photonic crystals in solar cells: the case of amorphous silicon," J. Opt. **14**(2), 024011 (2012).
33. S. E. Han and G. Chen, "Optical absorption enhancement in silicon nanohole arrays for solar photovoltaics," Nano Lett. **10**(3), 1012–1015 (2010).
34. Y. M. Song, S. J. Jang, J. S. Yu, and Y. T. Lee, "Bioinspired parabola subwavelength structures for improved broadband antireflection," Small **6**(9), 984–987 (2010).
35. D. G. Stavenga, S. Foletti, G. Palasantzas, and K. Arikawa, "Light on the moth-eye corneal nipple array of butterflies," Proc. Biol. Sci. **273**(1587), 661–667 (2006).
36. S. Collin, "Nanostructure arrays in free-space: optical properties and applications," Rep. Prog. Phys. **77**(12), 126402 (2014).
37. D. Maystre, "Theory of Wood's Anomalies," in *Plasmonics*, S. Enoch, and N. Bonod, eds. (Springer 2012), pp.39–83.
38. L. Rayleigh, "III. Note on the remarkable case of diffraction spectra described by Prof. Wood," Philos. Mag. Ser. 6 **14**(79), 60–65 (1907).
39. A. Hessel and A. A. Oliner, "A New Theory of Wood's Anomalies on Optical Gratings," Appl. Opt. **4**(10), 1275 (1965).
40. S. A. Boden and D. M. Bagnall, "Tunable reflection minima of nanostructured antireflective surfaces," Appl. Phys. Lett. **93**(13), 133108 (2008).
41. F. Wang, H. Yu, J. Li, X. Sun, X. Wang, and H. Zheng, "Optical absorption enhancement in nanopore Textured-Silicon Thin Film for Photovoltaic Application," Opt. Lett. **35**(1), 40–42 (2010).
42. J. Michel and L. C. Kimerling, "Design of Highly Efficient Light-Trapping Structures for Thin-Film Crystalline Silicon Solar Cells," IEEE Trans. Electron Dev. **54**(8), 1926–1933 (2007).
43. P. Spinelli, M. A. Verschuuren, and A. Polman, "Broadband omnidirectional antireflection coating based on subwavelength surface Mie resonators," Nat. Commun. **3**, 692 (2012).
44. Z. Y. Wang, R. J. Zhang, S. Y. Wang, M. Lu, X. Chen, Y. X. Zheng, L. Y. Chen, Z. Ye, C. Z. Wang, and K. M. Ho, "Broadband optical absorption by tunable Mie resonances in silicon nanocone arrays," Sci. Rep. **5**, 7810 (2015).

#261695 Received 22 Mar 2016; revised 8 May 2016; accepted 11 May 2016; published 25 May 2016

45. S. Kalem, P. Werner, B. Nilsson, V. G. Talalaev, M. Hagberg, O. Arthursson, and U. Södervall, "Controlled thinning and surface smoothening of silicon nanopillars," Nanotechnology **20**(44), 445303 (2009).
46. H. Toyota, K. Takahara, M. Okano, T. Yotsuya, and H. Kikuta, "Fabrication of microcone array for antireflection structured surface using metal dotted pattern," Jpn. J. Appl. Phys. **40**(7B), 5–8 (2001).
47. I. Suemune, H. Nakajima, X. Liu, S. Odashima, T. Asano, H. Iijima, J.-H. Huh, Y. Idutsu, H. Sasakura, and H. Kumano, "Metal-coated semiconductor nanostructures and simulation of photon extraction and coupling to optical fibers for a solid-state single-photon source," Nanotechnology **24**(45), 455205 (2013).
48. K. Han, J. Shin, W. Yoon, and H. Lee, "Enhanced performance of solar cells with anti-reflection layer fabricated by nano-imprint lithography," Sol. Energy Mater. Sol. Cells **95**(1), 288–291 (2011).
49. J.-W. Ho, Q. Wee, J. Dumond, A. Tay, and S.-J. Chua, "Versatile pattern generation of periodic, high aspect ratio Si nanostructure arrays with sub-50-nm resolution on a wafer scale," Nanoscale Res. Lett. **8**(1), 506 (2013).
50. X. Chen, Z. Fan, Y. Xu, G. Song, and L. Chen, "Microelectronic Engineering Fabrication of biomimic GaAs subwavelength grating structures for broadband and angular-independent antireflection," Microelectron. Eng. **88**(9), 2889–2893 (2011).
51. K. Hadobas, S. Kirsch, A. Carl, M. Acet, and E. F. Wassermann, "Reflection properties of nanostructure-arrayed silicon surfaces," Nanotechnology **11**(3), 161–164 (2000).
52. J. W. Leem, Y. M. Song, and J. S. Yu, "Six-fold hexagonal symmetric nanostructures with various periodic shapes on GaAs substrates for efficient antireflection and hydrophobic properties," Nanotechnology **22**(48), 485304 (2011).
53. R. Sanatinia, K. M. Awan, S. Naureen, N. Anttu, E. Ebraert, and S. Anand, "GaAs nanopillar arrays with suppressed broadband reflectance and high optical quality for photovoltaic applications," Opt. Mater. Express **2**(11), 1990–1995 (2012).
54. H. Xu, N. Lu, D. Qi, J. Hao, L. Gao, B. Zhang, and L. Chi, "Biomimetic antireflective Si nanopillar arrays," Small **4**(11), 1972–1975 (2008).
55. S. Naureen, R. Sanatinia, N. Shahid, and S. Anand, "High optical quality InP-based nanopillars fabricated by a top-down approach," Nano Lett. **11**(11), 4805–4811 (2011).
56. Y. Li, J. Zhang, S. Zhu, H. Dong, F. Jia, Z. Wang, Y. Tang, L. Zhang, S. Zhang, and B. Yang, "Bioinspired silica surfaces with near-infrared improved transmittance and superhydrophobicity by colloidal lithography," Langmuir **26**(12), 9842–9847 (2010).
57. H. Park, D. Shin, G. Kang, S. Baek, K. Kim, and W. J. Padilla, "Broadband optical antireflection enhancement by integrating antireflective nanoislands with silicon nanoconical-frustum arrays," Adv. Mater. **23**(48), 5796–5800 (2011).
58. X. Zhang, J. Zhang, Z. Ren, X. Li, X. Zhang, D. Zhu, T. Wang, T. Tian, and B. Yang, "Morphology and wettability control of silicon cone arrays using colloidal lithography," Langmuir **25**(13), 7375–7382 (2009).
59. C. M. Hsu, S. T. Connor, M. X. Tang, and Y. Cui, "Wafer-scale silicon nanopillars and nanocones by Langmuir-Blodgett assembly and etching," Appl. Phys. Lett. **93**(13), 33109 (2008).
60. W.-L. Min, B. Jiang, and P. Jiang, "Bioinspired Self-Cleaning Antireflection Coatings," Adv. Mater. **20**(20), 3914–3918 (2008).
61. W.-L. Min, P. Jiang, and B. Jiang, "Large-scale assembly of colloidal nanoparticles and fabrication of periodic subwavelength structures," Nanotechnology **19**(47), 475604 (2008).
62. C.-H. Sun, P. Jiang, and B. Jiang, "Broadband moth-eye antireflection coatings on silicon," Appl. Phys. Lett. **92**(6), 061112 (2008).
63. K. S. Han, H. Lee, D. Kim, and H. Lee, "Fabrication of anti-reflection structure on protective layer of solar cells by hot-embossing method," Sol. Energy Mater. Sol. Cells **93**(8), 1214–1217 (2009).

1. Introduction

For decades, in order to improve solar-cell efficiency, diverse photonic designs have been proposed [1]. Thin film crystalline silicon solar cells are considered to be one of the promising techniques due to fabrication cost and the abundance. However, the relatively low light absorption in the red and near-infrared wavelength ranges limits the efficiency of thin film solar cells [2–4]. Therefore, effective light trapping designs are mandatory to develop the efficiency of thin film solar cells. Several light trapping schemes by using a metal back reflector [5] or managing incident light efficiently [2,6] have been designed. Recently, nanostructure arrays such as nanopillar, nanowire and nanocone arrays enhancing light trapping [7–15], broadband optical absorption with tunable Mie resonance [16,17] and anti-reflecting structures based on sub-wavelength (SWS) with a tapered feature, called "moth-eye" which diminish unnecessary surface reflections [18–25] have also been exploited. These nanostructure arrays can be utilized to reduce reflectance and enhance absorption in solar cells without adding extra materials. Although various structures have been developed to enhance efficiency of thin film solar cells, there are relatively few researches on geometrical

#261695 Received 22 Mar 2016; revised 8 May 2016; accepted 11 May 2016; published 25 May 2016

comparison between a regular square array of nanorod (cylindrical-shaped) [12] and a tapered submicron structure with a graded index profile [18].

This report aims to address the above question by demonstrating our recent progress on designing and analyzing different light trapping structures, i.e., rod and paraboloid arrays and a structure transformed between these two devices by depending on parabolic ratio (will be discussed in Fig. 4) based on crystalline silicon (*c*-Si) [26] and gallium arsenide (GaAs) [27]. We numerically investigated the effect of the optimum shape on efficiency of solar cells by varying total cell thickness. In the process, other optimum parameters of structures such as period, height and filling fraction will be also discussed. According to our results, efficiency of the structure with a thickness of 500 nm, where both rod and paraboloid cells show the similar tendency in terms of cell efficiency and reflectance, is maximized with a truncated parabola-shaped array. This shape is also known as conical frustum shape or truncated cone in other papers [15,28,29] and defined as the structure with a parabolic ratio of 50% in our paper. We then show the diverse fabrication methods to ensure reproducibility and controllability of the proposed structures.

2. Optical design of structures and methods

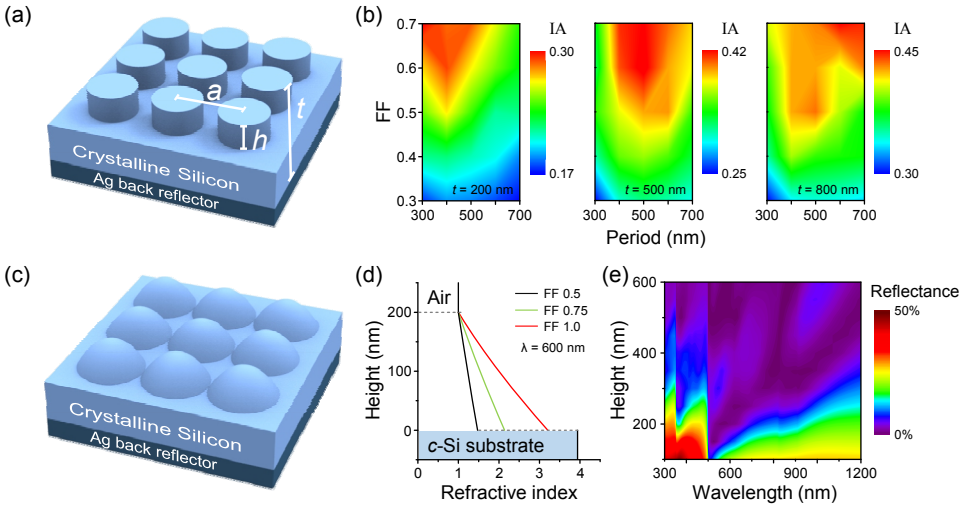

Fig. 1. Schematic view of thin-film *c*-Si solar cells (a) with rod array and characteristic parameters and (c) parabola array. (b) Contour maps of the integrated absorption as a function of the period of the rod arrays and their FF with various cell thicknesses. (d) Calculated effective refractive indice of the parabola arrays with three different FFs corresponding to the height. (e) Contour map of the variation of surface reflectance as a function of wavelength for the parabola structure and its height.

Figures 1(a) and 1(c) illustrate the configurations of *c*-Si thin film solar cells with rod and paraboloid arrays, respectively, from the top in air. A square symmetry has been chosen and the structures are defined by following factors: lattice period *a*, height of nano-patterned structure *h,* filling fraction FF defined by particle diameter / lattice period *a* and total cell thickness *t* which includes *h* as shown in Fig. 1(a). In our design, a silver (Ag) [30] metal back reflector is incorporated onto the bottom side for enhancing light trapping. Although Ag requires relatively higher cost than Al, it was selected for high absorption characteristic of solar cells. We use simulation study to examine how geometrical shape influences efficiency of thin-film *c*-Si solar cells using rigorous coupled wave analysis (RCWA) implemented by the commercial software package (DiffractMOD, Rsoft, USA) taking into account the AM1.5G solar spectrum. The direction of incident light is normal to the nanostructures unless otherwise specified and we considered the wavelength range varying from 300 nm to 1200 nm which covers the major solar energy spectrum. Zero to fifth diffraction orders were

#261695 Received 22 Mar 2016; revised 8 May 2016; accepted 11 May 2016; published 25 May 2016

considered to calculate the diffraction efficiency, which is enough to numerically stabilize our results.

As demonstrated in Fig. 1(b), scanning period and FF was performed for rod arrays to obtain the optimum parameters, resulting in maximizing the integrated absorption (IA) efficiency since these two parameters significantly affect the absorption characteristics of *c*-Si thin film solar cells [31]. These calculations were conducted over a technologically reasonable range: between 300 and 700 nm for period and 0.3 to 0.7 for FF [32] with three different thicknesses (i.e., h = 100 nm for t = 200 nm, h = 200 nm for t = 500 nm and h = 400 nm for t = 800 nm). As can be seen, regions characterized by a high IA are observed around a FF of 0.7 for all cases, therefore, it is attributed to the fact that a subtle change in the parameters hardly influence the optical properties of our structures. In this regard, we fixed the value of FF for our rod structures as 0.7 which is also a practical value to gain high performance solar cells [33].

Figure 1(d) shows the change of the effective refractive index, calculated with the volume weighted average refractive index of air (n_{air} = 1) and *c*-Si ($n_{c\text{-}Si}$ ~3.94 at a wavelength of 600 nm), of the same paraboloid structures but different FF corresponding to the height. For the cases of FF 0.5 and 0.75, the lines are steeper than the case of FF 1.0. This means that the refractive indice of these nanostructures more abruptly change at the interface between substrate and nanostructure, resulting in degrading the anti-reflection (AR) property of cells. However, the effective refractive index of the paraboloid structure with a FF of 1 more gradually increases as the height is more adjacent to the substrate. This case thus is the most viable solution among our paraboloid structures in terms of FF to reduce the Fresnel reflection [34,35], providing the improvement of solar cell efficiency. Therefore, FF is always set equal to 1 for our paraboloid structures.

Figure 1(e) illustrates simulated surface reflectance of the paraboloid nanostructure as a function of wavelength with following parameters: height is varied from 100 nm to 600 nm with a period of 500 nm. The total cell thickness is negligible for this case since the back reflection which occurs between Ag reflector and *c*-Si substrate was not considered to analyze how height influences the reflectance of the paraboloid structure. Higher order diffraction losses are observed in the wavelength range below ~500 nm. An abrupt change of the reflectance at the wavelength of about 350 nm is caused by transition of density distribution of the diffraction orders. At the wavelength of 500 nm which is analogous to the period of the structure, the drastic decrease of reflectance occurs due to Wood-Rayleigh (WR) anomaly from the grating formed by the regular array of nanoparticles, providing the cut-off high orders [36–39]. In the wavelength range above ~500 nm, the AR performance is gradually improved as the height is increased and saturated beyond a height of around 400 nm. These phenomena are explained by the fact that if a height is not tall enough, the effective refractive index abruptly appears to the incoming light [18,34,40]. This also indicates that in order to properly implement the AR property in the visible and near-infrared region, a height should be at least around 200 nm.

3. Result and discussion

In order to investigate how geometrical shape influences efficiency of solar cells as the cell thickness is increased, we performed a number of simulations for the two cases of array with varying height and period since these two parameters which strongly affect the absorption characteristics should be considered to achieve high cell efficiency in *c*-Si solar cells [33,41].

Cell efficiency was calculated by the equation:

$$\eta = J_{sc} V_{oc} \Gamma_f / P_{in,} \tag{1}$$

where J_{sc} is the short-circuit current density, V_{oc} is the open-circuit current, Γ_f is the filling factor and P_{in} is the total incident power under the AM1.5G solar spectrum. In our calculation, the collection efficiency of 85% with a 5% shadowing effect from the electrode was used. The reverse bias saturation current was taken to be $1.5\times10^{-15}\, A/cm^2$, and the

#261695 Received 22 Mar 2016; revised 8 May 2016; accepted 11 May 2016; published 25 May 2016

filling factor was fixed to 80%. The details of the used procedure can be found in the literature [42].

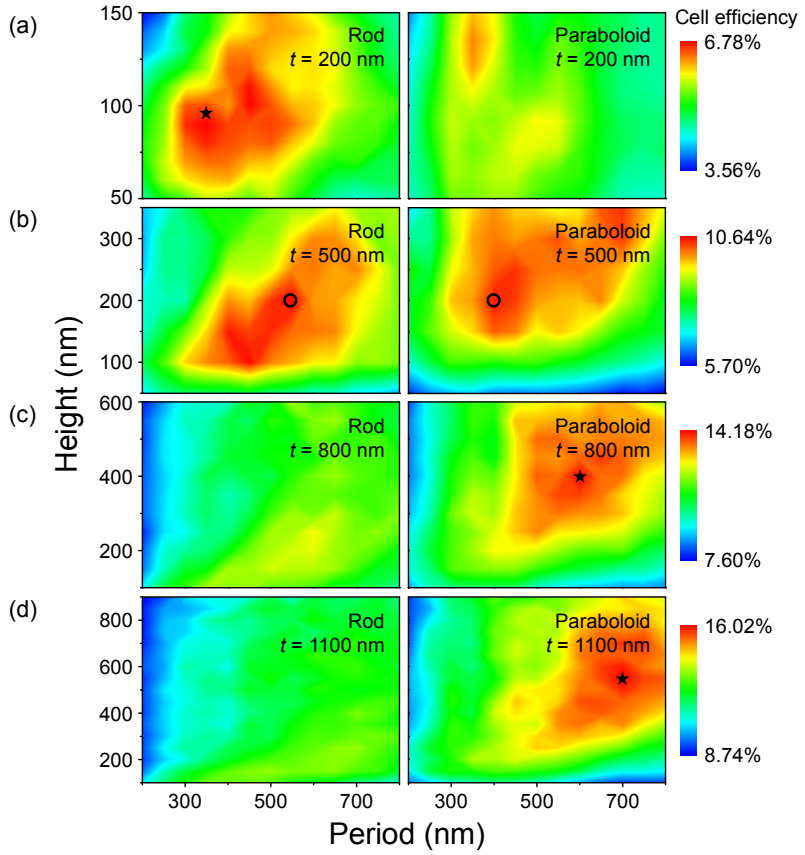

Fig. 2. Simulated cell efficiencies versus height and period contour plots for cell thicknesses of (a) 200 nm, (b) 500 nm, (c) 800 nm and (d) 1.1 μm with rod and parabola array structures.

Figure 2 demonstrates the calculated cell efficiencies versus period varying from 200 nm to 800 nm and variations in height depending on total cell thickness contour plots for *t* of 200 nm, 500 nm, 800 nm and 1100 nm with rod and paraboloid structures. For the cases whose *t* are 200 nm shown in Fig. 2(a), the nanorod one has the maximum cell efficiency (6.78%, 45.7% boosted comparing to the case of flat surface) depicted as a star sign with a period of 350 nm and a height of 90 nm. The optimum periods and heights of the *c*-Si thin films with *t* of 800 nm and 1100 nm are 600 nm and 400 nm with parabola-shaped and 700 nm and 550 nm with also parabola-shaped, respectively, shown in Figs. 2(c) and 2(d). The maximum cell efficiencies of 800 nm and 1100 nm cells are 14.18% and 16.02%, 42.6% and 43.6% improved comparing to their flat surface cells.

Interestingly, a thickness of 500 nm shown in Fig. 2(b), the highest values of cell efficiencies of both rod and paraboloid structures are nearly the same and depicted as circle symbols, 10.64% with h = 200 nm, a = 550 nm and 10.52% with h = 200 nm, a = 400, respectively. This is expected to the fact that another optimum shape for maximizing efficiency may exist and this work will be justified in Fig. 4. Structures thicker than 800 nm such as 1100 nm in Fig. 3(d) and 2 μm, which is not shown in this paper but calculated, have optimum values with paraboloid surface. This tendency is attributed the fact that the heights are tall enough to properly implement the AR property in paraboloid structures, resulting in enhancing absorption characteristic of solar cells, which is previously mentioned in Fig. 1(e).

#261695 Received 22 Mar 2016; revised 8 May 2016; accepted 11 May 2016; published 25 May 2016

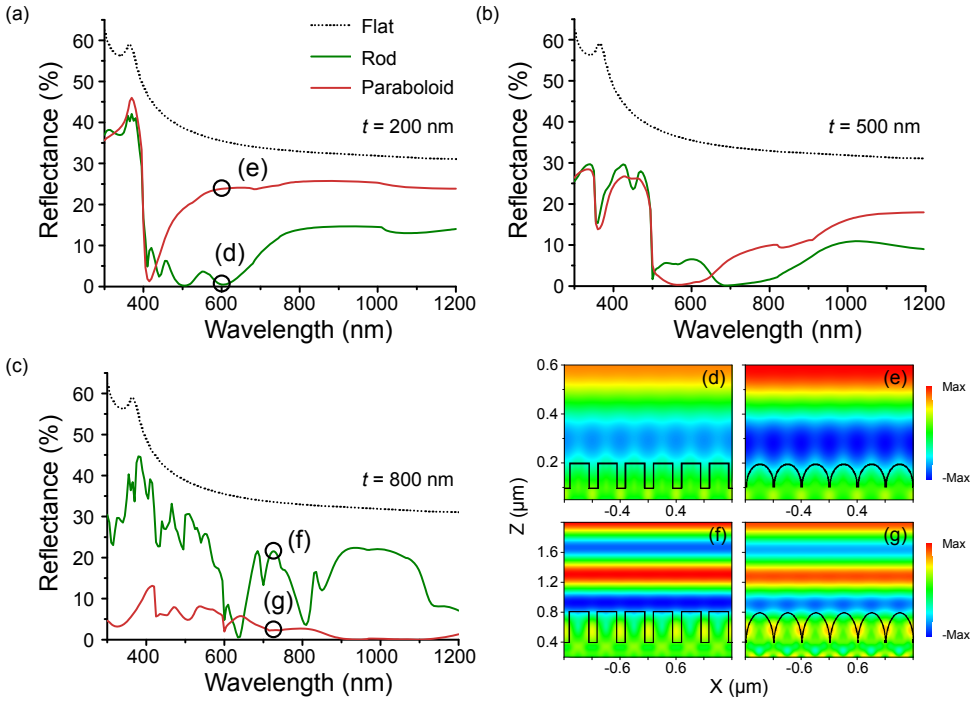

Fig. 3. Simulated surface reflection spectra from structures with flat (black), Rod- (green) and Parabola-shaped (red), for cell thicknesses of (a) 200 nm, (b) 500 nm and (c) 800 nm with mentioned height and period. Electric field distributions of the structures (d), (e) at the wavelength of 600 nm and (f), (g) 710 nm shown in [Figs. 3(a) and 3(c)] as the circle symbols.

To understand these mechanisms, as shown in Fig. 3, the reflectance spectra of nano-patterned surfaces without back reflection were performed in the visible and near-infrared region as the total cell thickness is increased with following heights and periods: (a) h = 100 nm, a = 400 nm and these are slightly adjusted from the optimum values due to difficulties in fabrication, (b) h = 200 nm, a = 500 nm and these are reasonably overlapping values, almost the mean value of the optimum parameters for both structures in Fig. 2(b), 2(c) h = 400 nm, a = 600 nm. We also calculated the reflectance of a flat surface for comparison. In Fig. 3(a), despite the fact that the dips of reflection resulting from the WR anomaly occur in both structures at a wavelength of 400 nm which is equivalent to the period, the reflectance of the rod-shaped one is still far lower than that of paraboloid one. This is because in the wavelength range above ~400 nm, dips are clearly observed due to optical resonances, which are specific to the square rod arrays and depend on aspect ratio and period of structures. These mutually adjacent dips and the WR anomaly consequently broaden the AR property. Mie resonance which redshifts for increasing particle diameter is also observed at a wavelength of 1100 nm since the diameter of the particle is 280 nm resulted from a FF of 0.7 and a period 400 nm) [43,44]. However, due to the fact that this property weakly appears and c-Si has low light absorption in the region (~1100 nm), this result hardly affects the efficiency of solar cells. For the case of paraboloid, although the parabola-shaped one is a sub-wavelength structure (SWS) in the wavelength range above ~400 nm, which requires dimension smaller than the optical wavelength, and exhibits a linearly graded index profile, the AR property is weakly observed since the height is not tall enough to proceed the AR property in the broadband wavelength range as previously mentioned in Fig. 1(e). The electric field distributions in Figs. 3(d) and 3(e) provide useful information for understanding the reflectance on the surfaces. In Fig. 3(b), the reflectance of both structures are remarkably

#261695 Received 22 Mar 2016; revised 8 May 2016; accepted 11 May 2016; published 25 May 2016

similar in the range of below ~500 nm and the sharp dips at a wavelength of about 500 nm are consistent with the WR anomaly. Above ~500 nm, although the rod one is slightly more practical than the paraboloid one in terms of the AR property, it is hard to assert that the former is more viable than the latter as there is only a subtle improvement.

As depicted in Fig. 3(c), the paraboloid structure with a cell thickness of 800 nm exhibits a high performance of the AR property in the broadband spectrum. The light with the wavelengths greater than 600 nm, the structure is a SWS which suppresses the Fresnel reflection at the interface between air and surface due to the gradually increasing refractive index. Although the rod structure shows dips of reflectance, the paraboloid one shows the far more effective AR property. These results therefore indicate that, in effective medium theory, the paraboloid structure can considerably reduce the surface reflection and additionally, be efficient to achieve a high broadband absorption. The electric field distributions are also simulated in Figs. 3(f) and 3(g). The result displays that the AR property of the paraboloid structure is visible compared to the rod one.

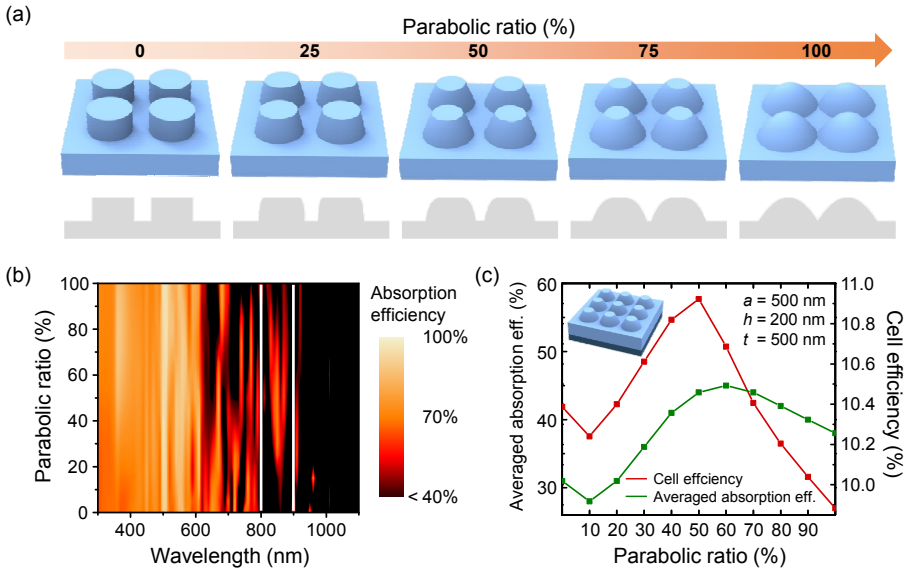

Fig. 4. (a) Geometrical transformation process of nanostructure shape by varying parabolic ratio. (b) Contour map of the variation of absorption efficiency as a function of wavelength for the thin-film *c*-Si solar cell and its parabolic ratio (Only absorption efficiency above 40% are plotted). (c) Calculated cell efficiency of the *c*-Si solar cell (red) and averaged absorption efficiency (green) over the range of wavelength 800-900 nm depicted as a white rectangular in Fig. 4(c) as a function of the parabolic ratio. Inset: Schematic view of a PR50% patterned thin-film *c*-Si solar cell.

In order to provide further insight into the case of 500 nm thickness where both rod and parabola arrays show the almost equal values of cell efficiencies and the similar reflectance characteristics, we conducted more simulations by transforming shape of the nanostructures. A simple quadratic function is used to describe the variations in parabolic ratio of the structures. The function was designed on the basis of the tapered function of paraboloid. To obtain gradual change of geometrical shape from rod to paraboloid, the tapered order (TO) was defined by the parabolic ratio raised to the power of 1.5.

$$Tapered\ order\ (TO) = (Parabolic\ ratio)^{1.5} \tag{2}$$

The equation of describing paraboloid raised to the power of the tapered order describes parabolic ratio of structures. The final equation is defined as:

#261695 Received 22 Mar 2016; revised 8 May 2016; accepted 11 May 2016; published 25 May 2016

$$f(z) = 1 - (1 - z)^{\frac{1}{2} \times TO} \quad (3)$$

In this equation, the range of 'z' value is limited to from 0 to 1, normalized values of heights.

Figure 4(a) illustrates the geometrical transformation process of nanostructure shape. For instance, if the ratio is 100%, a surface is composed of parabola-shaped nanostructure whereas 0% of parabolic ratio means that the structure is perfect rod-shaped one. Figure 4(b) demonstrates simulated absorption efficiency as a function of the wavelength and parabolic ratio with following factors (a = 500 nm, h = 200 nm and t = 500 nm). The result shows that, in the spectral range 800–900 nm in which c-Si has low light absorption depicted as a white rectangular in Fig. 4(b), the absorption efficiencies of the structures with parabolic ratio range 40-80% are higher than both pure rod and paraboloid ones whose parabolic ratio are 0% and 100%, respectively. The averaged values of this result is also shown as a line graph (green) in Fig. 4(c). In this regard, this tendency can be worth being studied since the efficiency of thin-film c-Si solar cells strongly depends on optical absorption. Only absorption efficiency above 40% are plotted to highlight the differences of absorption efficiencies among the structures. Further simulation was carried out to analyze the effect of the parabolic ratio.

Calculation of cell efficiency was conducted as the parabolic ratio is increased demonstrated as a line graph (red) in Fig. 4(c). The peak value of cell efficiency is observed at a parabolic ratio of 50%, therefore, this result is expected to the fact that the structure whose parabolic ratio is 50% may possess combined benefits from both rod and paraboloid structures. It also means that in order to maximize the performance of solar cells, a geometrical shape should be considered in a given thickness.

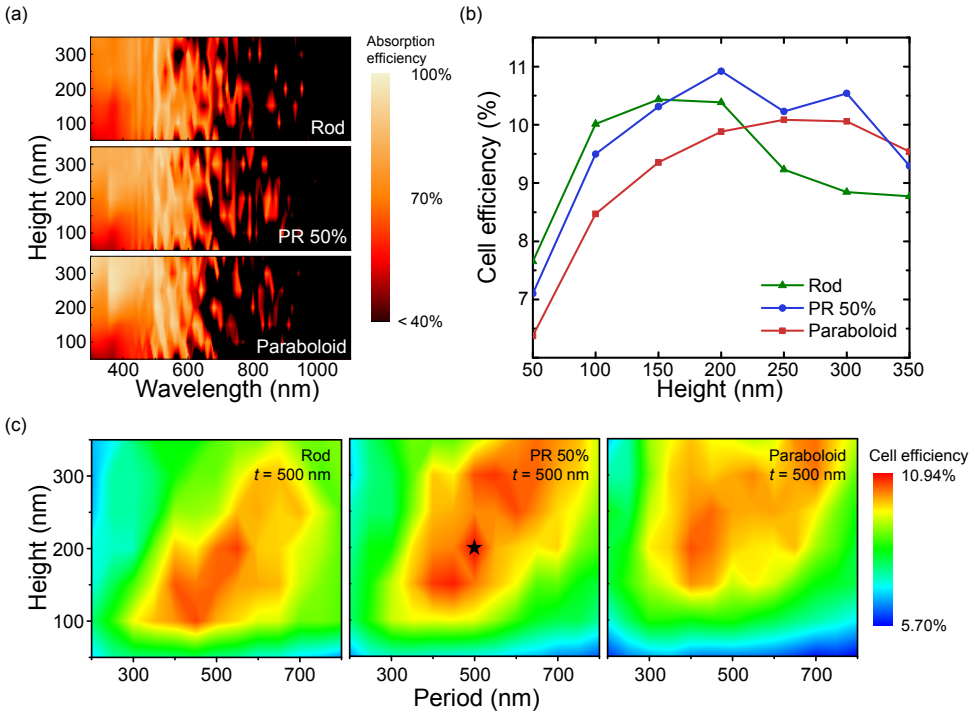

Fig. 5. (a) Absorption efficiency in function of the wavelength and height of the c-Si thin films with three different light-trapping structures (Only absorption efficiency above 40% are plotted). (b) Calculated cell efficiency of the structures as a function the height. (c) Cell efficiencies versus height and period contour plots for cell thickness of 500 nm with varying the shape of nanostructures.

#261695 Received 22 Mar 2016; revised 8 May 2016; accepted 11 May 2016; published 25 May 2016

To ensure the fact that the nanostructure patterned with PR 50% is more adequate for maximizing cell efficiency than both conventional rod and paraboloid structures for the case of a cell thickness of 500 nm, diverse simulations were conducted with a period of 500 nm. Figure 5(a) shows the simulated absorption efficiency for the three different light trapping structures with heights varying from 50 nm to 350 nm. The noticeable increase of absorption efficiency for all structures at the wavelength of 500 nm, which is equal to lattice period *a*, is observed due to the WR anomaly. The paraboloid one not only has WR anomaly, but also shows that the higher absorption efficiencies can be obtained at the taller heights. The reason is already mentioned in Fig. 1(e). However, this structure exhibits relatively low absorption efficiency in the red and near-infrared region compared with other two devices. As can be seen, as a whole, PR 50% is expected to partly have the advantages of both rod and paraboloid structures. To further understand this, Fig. 5(b) demonstrates the calculated cell efficiency of the three light trapping structures as a function of the height. The optimum heights of rod and palaboloid in order to obtain the maximum cell efficiency are 150 nm and 250 nm, respectively, corresponding to a period of 500 nm. As we expected, PR 50% has the maximum cell efficiency with a height of 200 nm which is the middle point of optimum heights of the other two structures. In order to consider periods of the structures, additional simulations were carried out. In Fig. 5(c), PR 50% shows the highest performance with a cell thickness of 500 nm which is the exactly median value of 200 nm optimized by rod-shaped and 800 nm optimized by parabola-shaped shown in Figs. 2(a) and 2(c). 10.94% of cell efficiency is achieved, 46% boosted comparing to the structure with flat surface.

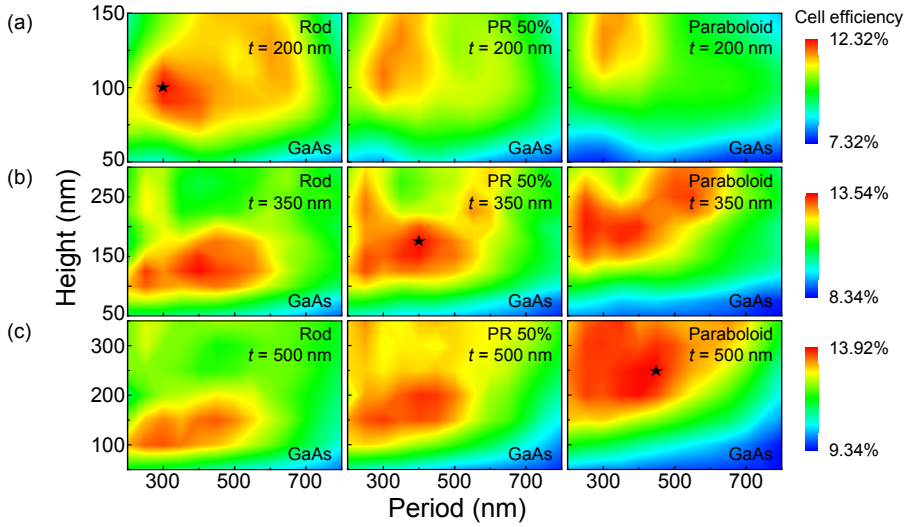

Fig. 6. Simulated cell efficiencies for GaAs versus height and period contour plots for cell thicknesses of (a) 200 nm, (b) 350 nm and (c) 500 nm with three different light trapping structures.

To study further the effect of geometrical shape on solar cells, we conducted simulations using GaAs which is widely used in high-efficiency photovoltaics and other devices. The result shown in Fig. 6 exhibits the fact that the highest cell efficiencies of solar cells based on GaAs also depend on geometrical shape as the cell thickness is increased. The PR 50% structure has the maximum cell efficiency with a cell thickness of 350 nm, which is the exactly median value of 200 nm and 500 nm. However, the tendency is more sensitive than the cases of solar cells based on *c*-Si. This is explained by the fact that although the cell thicknesses are thinner than *c*-Si based solar cells, which reduce optical path length in substrate, high extinction coefficient of GaAs [4] dominantly affects the tendency. This is far from ideal for achieving the maximum cell efficiency of solar cells owing to the sensitivity of

#261695 Received 22 Mar 2016; revised 8 May 2016; accepted 11 May 2016; published 25 May 2016

the optimum shape to slight changes in cell thicknesses. Also, the gaps of the maximum values among the structures with different thicknesses are small-scale compared to the structures based on *c*-Si. It is therefore inadequate to consider the optimum geometrical shape for maximizing the performance of GaAs solar cells. In this regard, studying with this concept for other material used for solar cells is worth taking into account to decide whether scanning the optimum shape for maximizing efficiency of photovoltaics is meaningful or not.

In order to provide insight into applicability of proposed structures to photovoltaic systems in reality, fabrication methods should be considered. Recently, patterning process to form etching mask is conducted by a variety of techniques such as e-beam lithography [19,45–47], nanoimprint lithography [21,22,25,48,49], interference lithography [18,23,34,50–52] and colloidal lithography [8,13,15,20,53–62]. Geometrical shape of structures strongly depends on etching condition and selection of etching gases [56–59]. Degree of tapering on structures toward paraboloid or cone can be normally adjusted by etching selectivity and control of undercut. Truncated structures, described with parabolic ratio in our paper, have also been reported in similar ways [47,52–59]. Diverse fabrication methods for proposed structures and practicability to different materials are summarized in Table 1. to ensure the reproducibility and controllability. Previously reported results have been showing noticeable performance and support the feasibility of our structures on photovoltaic applications.

Table 1. Fabrication methods of rod, paraboloid, and truncated structure

Structure	Fabrication method	Material	Ref.
Rod	Interference lithography, Reactive ion etching	Si	[51]
	Colloidal lithography, Reactive ion etching	Si	[13,15,59–62]
	Nanoimprint lithography, Reactive ion etching	Si	[49]
	Electron beam lithography, Inductively coupled plasma / reactive ion etching	Si	[45]
	Selective area epitaxy, Metal organic chemical vapor deposition	GaAs	[14]
Paraboloid	Interference lithography, Inductively coupled plasma etching	Si, GaAs	[18,23,34,50,52]
	Colloidal lithography, Reactive ion etching	Si	[8,20,58]
	Nanoimprint lithography, Reactive ion etching	Si	[21,22,25,48]
	Electron beam lithography, Fast atom beam / reactive ion etching	Si, SiO_2	[19,46]
	Hot embossing method	PVC	[63]
Truncated structure	Interference lithography, Inductively coupled plasma etching	GaAs	[52]
	Colloidal lithography, Reactive ion etching	Si, SiO_2, GaAs	[53–59]
	Electron beam lithography, Inductively coupled plasma / reactive ion etching	InP, GaAs	[47]

4. Conclusions

In summary, *c*-Si nanostructures with various shapes were investigated by simulations. Our studies indicate that the maximum cell efficiency of structures depends on their geometrical shapes as the total cell thickness is increased. The calculated reflectances reveal that the AR property should be considered to design high performance solar cells. The results demonstrate that for the case of ultrathin solar cell with a thickness of 200 nm, a rod-shaped structure can be an appropriate design due to optical resonances from the optimum

#261695 Received 22 Mar 2016; revised 8 May 2016; accepted 11 May 2016; published 25 May 2016

parameters. The PR 50% thin film *c*-Si solar cell can be used to maximize the cell efficiency with a cell thickness of 500 nm. With increasing thickness more than 800 nm, a parabola-shaped structure can be more applicable than other structures owing to the effective graded index profile, resulting in the entire AR performance. In this regard, in order to obtain the highest performance for solar cells, it is crucial to determine the optimum geometrical shape of structures in a given thickness. The dependence of geometrical shape on cell thickness can provide useful controlling parameters in designing photovoltaic and optical devices.

Acknowledgments

W. I. Nam and Y. J. Yoo equally contributed to this work. This work was partly supported by the Basic Science Research Program of the National Research Foundation of Korea (NRF) funded by the Ministry of Science, ICT and Future Planning (2014R1A1A1005945), MSIP as GFP / (CISS-2013M3A6A6073718) and Pusan National University Research Grant, 2013.

#261695 Received 22 Mar 2016; revised 8 May 2016; accepted 11 May 2016; published 25 May 2016